

Ultrasonic Implant Localization for Wireless Power Transfer: Active Uplink and Harmonic Backscatter

Max L. Wang, Ting Chia Chang, Amin Arbabian
Department of Electrical Engineering, Stanford University, Stanford, CA, USA

Abstract—Efficient ultrasonic power transfer to implantable devices requires precise transmitter beamforming to the receiver and can quickly degrade with small changes in implant location. Ultrasound localization can be used to find and track implants in the body to maintain an efficient link. We present a framework to calculate localization accuracy showing that sub-mm accuracy is obtainable using only three receive channels. A harmonic backscatter approach, which passively provides contrast in the frequency domain without active load modulation is compared to active uplink from the implant. The localization accuracy using both active uplink and harmonic backscatter from the implant power receiver is characterized using a linear array probe. The measured location standard deviation is nearly two orders of magnitude smaller than the half-power beamwidth of the array focal spot. Finally, beamforming using the measured location information increases the available power by over $20\times$ compared to an unfocused beam.

Index Terms—ultrasonic wireless power transfer, beamforming, implant, real-time localization, harmonic backscatter

I. INTRODUCTION

Wirelessly powered implantable devices have opened up many new biomedical applications from gut microbiome sensing [1] to neuromodulation [2]. Ultrasound (US) wireless power transfer has been shown to be effective for mm-sized implants aiming to operate deep within tissue. US power transfer benefits from many of the same advantages as US imaging in the body, including low tissue attenuation (0.5-1.0 dB/cm/MHz), high safety limits (7.2 mW/mm^2) [3], and efficient focusing to mm-sized spots. In addition, the millimeter wavelength of US in the body allows for high transduction efficiency with a miniaturized piezoelectric receiver, conforming to the implant size constraints [4]. Our previous work analyzed and demonstrated the US link, showing that efficient power transfer is possible at depths $>5 \text{ cm}$ with focused radiation and large transmit aperture [4], [5]. However, the increased focusing efficiency that comes from using larger transmit apertures can also make the link more sensitive to the location of the implant receiver due to the small focus beamwidth.

Most previous demonstrations of US wireless powering, both in tissue phantom or *in vivo*, use unfocused US power transmitters or know the implant receiver location *a priori* to maintain a robust link. For example, in [1] a US-powered implantable gut biosensor was tested in a rat cecum across

This work was supported by the NIH NIBIB under award number R01EB025867, the NSF CAREER Award under award number ECCS-1454107, and the Dr. Robert Noyce Stanford Graduate Fellowship.

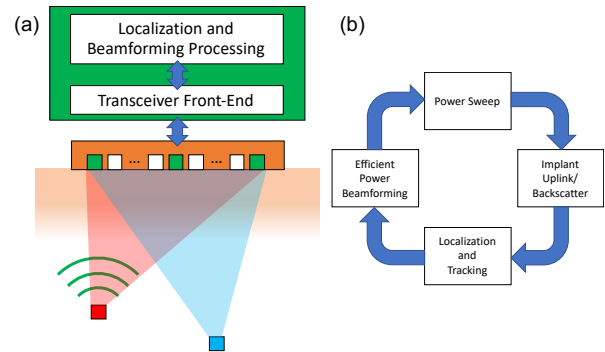


Fig. 1. (a) Conceptual diagram of the localization system showing power beamforming to the implants (red and blue) based on the signals received from only a few external receive channels (green). (b) Procedure to find and track implants for efficient beamforming.

multiple days. Since the location of the implant was only approximately known, a single-element unfocused US transducer (Olympus A303S) was used to ensure reliable power-up *in vivo* at the expense of power transfer efficiency.

Ultrasound can also be used to find and track implants for efficient power beamforming. US localization requires the implant to either actively transmit a pulse or backscatter a pulse that can be detected by external receivers (Fig. 1). US implant localization has recently been discussed in [6], [7] to increase the robustness of the link, but these works do not analyze localization accuracy. In addition, they consider systems in which all external array elements both transmit and receive, which can be difficult to implement in a wearable wireless powering system.

Here, we evaluate the expected localization accuracy of a power transfer system with only three receive elements, showing that it is sufficient to power implants both on and off-axis. We also describe a new technique for US localization using harmonic backscatter. Finally, we measure the localization precision and increase in power transfer using the measured implant location for beamforming.

II. LOCALIZATION ACCURACY

The efficiency of a US link depends on the focal spot size of the power transmitter. A focal spot that is similar in size to the implant receiver will improve the power link efficiency. On the other hand, a small focus means that slight movements between the transmitter and receiver can severely degrade the efficiency. For example, as detailed in [4], a 1 cm radius transmitter focused at 6 cm depth can have a

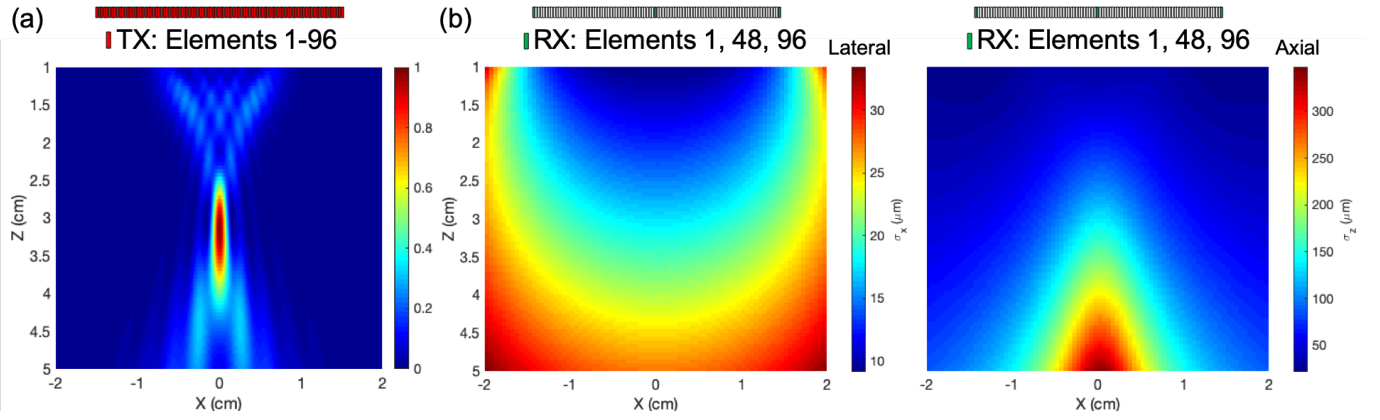


Fig. 2. (a) Simulated normalized intensity beam pattern of the P4-1 probe when focusing at 3 cm depth at 1 MHz. The beamwidth (1.6 mm lateral, 13.5 mm axial) sets the upper limit on localization accuracy. (b) The calculated lower bound on the location standard deviation in x (left) and z (right) with three receive channels (1, 48, and 96) for a 25 dB SNR signal with 600 kHz bandwidth.

focused half-power beamwidth of less than 3 mm around 2 MHz. Even slight static misalignments during transmitter or receiver placement or dynamic offsets from breathing could significantly change the powering efficiency.

In this work, we use a Philips P4-1 linear array probe as a power transmitter benchmark. This probe has 96 elements with $295 \mu\text{m}$ pitch resulting in an overall aperture of about 2.83 cm. A Field II simulation of the beam pattern when focused at 3 cm in a medium without attenuation is shown in Fig. 2(a) [8], [9]. The half-power beamwidth is about 1.6 mm along the x-axis and 13.5 mm along the z-axis. For robust powering, the localization accuracy needs to be well within these parameters, though the required accuracy for other applications can be much more stringent. Thus, it is worthwhile to calculate the attainable accuracy in an implant system.

Localization accuracy is related to imaging resolution in that it depends on the aperture of the array and bandwidth of the signal. Rather than considering the closest distance between two point sources that can still be resolved for imaging, localization depends on the accuracy in measuring the actual position of a target. Acoustic localization generally uses time of arrival (ToA) or time difference of arrival (TDoA) measurements along with a multilateration algorithm to determine location. Translating multiple ToA/TDoA measurements to a location estimate can be understood geometrically as the intersection of multiple circles/hyperbolas in two dimensions [10]. With noise, the intersection is no longer unique, and the problem can be formulated as a nonlinear optimization problem. For example, TDoA can be defined as

$$c\Delta t = f_{TDoA}(x) + n \quad (1)$$

$$f_{TDoA}(x) = \begin{bmatrix} \|x - x_2\| - \|x - x_1\| \\ \vdots \\ \|x - x_L\| - \|x - x_1\| \end{bmatrix} \quad (2)$$

where c is the speed of sound in the medium, Δt is the vector of measured TDoA between the different external

receivers, n is the measurement noise, L is the number of receivers, x is the location of the target, and x_{1-L} are the locations of the receivers.

We can define the cost function to optimize, J_{TDoA} , as

$$J_{TDoA} = \sum_{l=1}^L (c\Delta t_l - (\|x - x_l\| - \|x - x_1\|))^2. \quad (3)$$

The position estimate \hat{x} , can then be calculated by minimizing J_{TDoA} :

$$\hat{x} = \underset{\tilde{x}}{\text{argmin}} J_{TDoA}(\tilde{x}). \quad (4)$$

There are many ways to solve for \hat{x} with varying tradeoffs between time, complexity, and accuracy. Here, we use an iterative steepest descent algorithm.

The lower bound on the variance attainable by an unbiased estimator is given by the Cramer-Rao Lower Bound (CRLB). The CRLB for arrival time estimation is a function of SNR, observation time (T), and signal bandwidth (BW) [11]:

$$\sigma_{ToA}^2 \geq CRLB \propto \frac{1}{SNR \times T \times BW}. \quad (5)$$

The CRLB for the position estimate with three external receive elements can be calculated based on the position of the elements, position of the implant, and the time resolution. Fig. 2(b) shows the calculated lower bound for the standard deviation in position in both the lateral (x) and axial (z) dimensions across a $4 \text{ cm} \times 4 \text{ cm}$ powering window. At 3 cm depth on-axis, the lower bounds for the standard deviation are about $\sigma_x \geq 20 \mu\text{m}$ and $\sigma_z \geq 140 \mu\text{m}$. The minimum standard deviation can be seen to be nearly two orders of magnitude smaller than the half-power beamwidth of the focus from Fig. 2(a). Note that for localization in 3D space, a 2D array or movement of the array along the y-axis is needed.

III. ACTIVE UPLINK AND HARMONIC BACKSCATTER

Active uplink from an implant allows for separation in the time domain of the implant signal from power beam echoes.

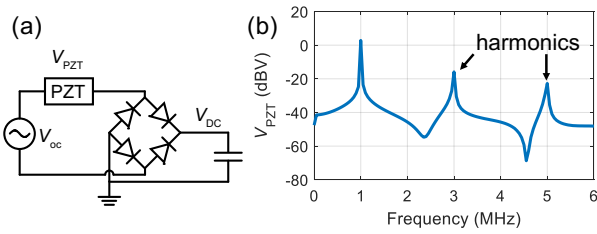


Fig. 3. (a) Basic circuit schematic of the power recovery from a piezo showing the full-wave rectifier and load capacitance. (b) The frequency spectrum of the voltage across the piezo impedance shows the odd harmonics generated by the rectifier nonlinearity.

However, it requires the implant to already have sufficient energy to transmit a pulse. While this can be achieved with an initial blind power sweep, passive options should also be considered. With passive backscatter, the main challenge is achieving contrast since there are many scatterers in tissue. In a conventional B-mode ultrasound image, an implant may not be discernible from other objects in the image. To achieve contrast, [6] either shorts or opens the connection to the implant PZT receiver, slightly changing the reflection over time in a deterministic way. This kind of method is common in RFID tags, but again requires the implant to charge prior to activating load modulation.

Rectification is a necessary component of the US power recovery chain, converting the received AC signal into a DC power that can be used by the implant (Fig. 3(a)). A rectifier presents a nonlinear load to the transducer, producing odd harmonics of the received signal. These harmonics, particularly the 3rd harmonic, will naturally be backscattered by the implant transducer. For example, for a 1 MHz power downlink, in addition to the fundamental, a 3 MHz signal will be backscattered. For the power levels transmitted in implant systems, the amount of 3rd harmonic naturally generated from tissue is negligible. Thus, the implant backscattered 3rd harmonic would provide contrast in the frequency domain without the additional load modulation circuits needed in conventional backscatter applications.

While the bandwidth at the 3rd harmonic may be greater than at the fundamental, the quality factor of the transducer and degree of nonlinearity also need to be considered. For a transducer that resonates at the fundamental of the power signal, the responsivity at the 3rd harmonic may be degraded. In addition, as can be seen in Fig. 3(b), the backscattered power at the harmonic will be lower than the fundamental. Both of these factors mean that the received SNR will ultimately be lower for harmonic backscatter compared to active uplink or conventional load modulation backscatter.

IV. LOCALIZATION RESULTS

Active uplink and harmonic backscatter measurements are performed using mm-sized PZT4 transducers (piezos) designed to resonate at 1 MHz as targets. These piezos represent the power receiving element for the implant. Two piezos (Piezo1 and Piezo2) are placed on top of two 0.2 mm thick PCBs in a tank filled with mineral oil, which has an acoustic

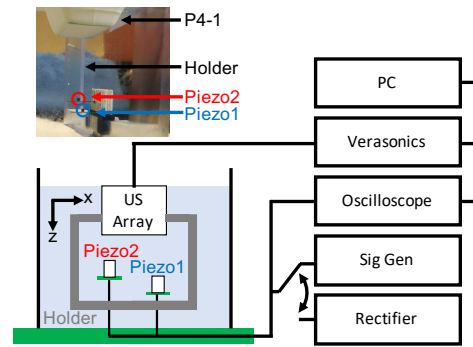


Fig. 4. Measurement setup to test the accuracy of active uplink and harmonic backscatter. A signal generator is used for active uplink and a rectifier circuit is connected externally for backscatter.

impedance similar to tissue. The piezos are spaced 10.2 mm apart in the x-dimension and 4 mm apart in the z-dimension. A Philips P4-1 96-element linear array probe is used for power transmission and signal reception. As can be seen in Fig. 4, the probe is centered by a rigid 3D-printed holder over the piezos. The overall electrical setup can also be seen in Fig. 4. All electronics are connected outside of the tank. The probe is controlled using a Verasonics Vantage 256 scanner (Verasonics Inc., Kirkland, WA). The piezo voltages are measured with an oscilloscope. For active uplink, a signal generator drives the piezos with a 4 V_{pp} signal. For harmonic backscatter, a full-wave rectifier, load capacitor, and load resistor are connected to the piezos.

For these experiments, only 3 probe elements (channels 1, 48, and 96) are used for receiving the uplink/backscatter signal. The location of the implants is calculated using (1) - (4). First, the signals are filtered around the signal carrier – 1 MHz for active uplink and 3 MHz for harmonic backscatter. One channel is designated as the reference. For each channel, the envelope is derived from the RF signal and cross-correlated with the reference to determine the TDoA. Note that the envelope is used rather than the RF signal to mitigate the effects of any phase offsets across the elements; these offsets could also be calibrated out with a known target location to increase accuracy. The target location is derived from solving (4) using an iterative steepest descent algorithm. The starting guess is calculated by converting (1) into a set of linear equations and using a one-step linear least squares solution.

Fig. 5 shows the calculated location from 200 measurements for Piezo1 and Piezo2 using both active uplink and harmonic backscatter. The location variance can be seen to be higher in the z-dimension than the x-dimension, as expected from the results shown in Fig. 2(b). The standard deviation in the location estimates are shown in Table I. Harmonic backscatter localization shows a larger spread than active uplink, but both the lateral and axial standard deviations are well within the half-power beamwidth of the focal spot generated by the P4-1 probe. The absolute location error is not calculated because the absolute location of the piezos is not known to micrometer-level accuracy. Nonetheless, the calculated relative separation between Piezo1 and Piezo2 is as expected.

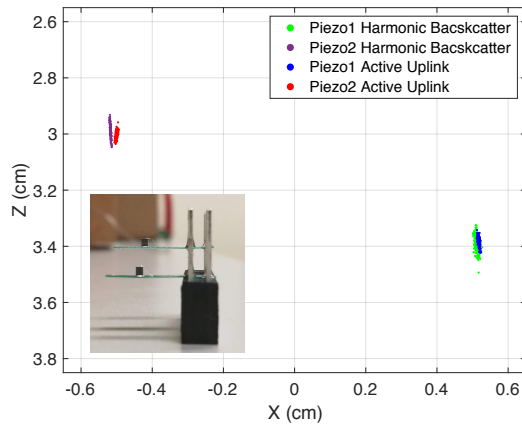


Fig. 5. Localization results for Piezo1 (right) and Piezo2 (left) after 200 receptions using both active uplink and harmonic backscatter. The results show the expected lateral separation of about 10.2 mm and axial separation of 4 mm. The spread in location estimates is larger for harmonic backscatter than for active uplink.

TABLE I
LOCATION STANDARD DEVIATION

$\sigma_{x,z}(\mu\text{m})$	Piezo1	Piezo2
Active Uplink		
Lateral	22.8	21.3
Axial	149	130
Harmonic Backscatter		
Lateral	45.7	13.8
Axial	268	236

Fig. 6 shows the power received by the piezos when 25 cycles of a $50 V_p$ 1 MHz signal is transmitted by all elements of the P4-1 probe. The unfocused power transfer shows an open-circuit voltage of about $1 V_p$ on both piezos, giving an available power of about $50 \mu\text{W}$. When directing the focus of the array to the calculated locations, the peak voltage increases to over $4.5 V_p$, increasing the available power by over $20\times$ to over 1 mW.

V. CONCLUSION

Efficient and robust power transfer requires knowledge of the implant location relative to the power transmitter. We review the fundamentals of localization processing and calculate the expected localization accuracy of our implant system. The concept of harmonic backscatter is introduced to passively achieve contrast from background tissue. Measurements using active uplink and passive harmonic backscatter are performed in mineral oil to quantify the localization accuracy. Finally, using the location for power beamforming increased the available power to the implant by over $20\times$. As we move toward *in vivo* localization and power beamforming, we can incorporate multipath correction, tracking, and 3D localization.

ACKNOWLEDGMENT

The authors would like to thank Professor Jeremy Dahl and his group for the use of their Verasonics Vantage system

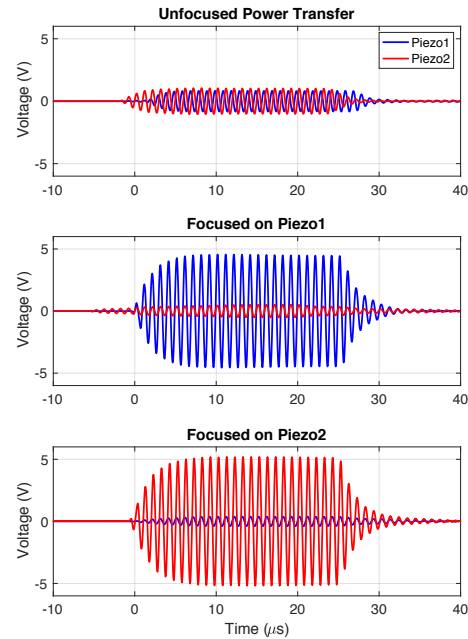


Fig. 6. Received voltage on Piezo1 and Piezo2 with an unfocused pulse (top) and focused pulse at the piezo locations. The available power increases by over $20\times$ when focusing at the calculated location.

as well as Dr. Arsenii Telichko, Dr. You Li, and Dr. Carl Herickhoff for valuable discussions.

REFERENCES

- [1] S. Baltasvius, W. Van Treuren, M. J. Weber, J. Charthad, S. Baker, J. L. Sonnenburg, and A. Arbabian, "In Vivo Wireless Sensors for Gut Microbiome Redox Monitoring," *arXiv:1902.07386*, Feb 2019.
- [2] J. Charthad, T. C. Chang, Z. Liu, A. Sawaby, M. J. Weber, S. Baker, F. Gore, S. A. Felt, and A. Arbabian, "A mm-Sized wireless implantable device for electrical stimulation of peripheral nerves," *IEEE Trans. Biomed. Circuits Syst.*, vol. 12, no. 2, pp. 257–270, 2018.
- [3] "Information for Manufacturers Seeking Marketing Clearance of Diagnostic Ultrasound Systems and Transducers," U.S. Department of Health and Human Services, Rockville, Tech. Rep., 2008.
- [4] T. C. Chang, M. J. Weber, J. Charthad, S. Baltasvius, and A. Arbabian, "End-to-end design of efficient ultrasonic power links for scaling towards submillimeter implantable receivers," *IEEE Trans. Biomed. Circuits Syst.*, vol. 12, no. 5, pp. 1100–1111, 2018.
- [5] M. L. Wang, T. C. Chang, T. Teisberg, M. J. Weber, J. Charthad, and A. Arbabian, "Closed-Loop Ultrasonic Power and Communication with Multiple Miniaturized Active Implantable Medical Devices," in *2017 IEEE International Ultrasonics Symposium (IUS)*, 2017.
- [6] Y. Zhang and K. L. Shepard, "A 0.6-mm² Powering and Data Telemetry System Compatible with Ultrasound B-Mode Imaging for Freely Moving Biomedical Sensor Systems," in *2019 IEEE Custom Integrated Circuits Conference (CICC)*, 2019, pp. 1–4.
- [7] M. Meng and M. Kiani, "Self-Image-Guided Ultrasonic Wireless Power Transmission to Millimeter-Sized Biomedical Implants," in *2019 41st Annual International Conference of the IEEE Engineering in Medicine and Biology Society (EMBC)*, 2019, pp. 364–367.
- [8] J. A. Jensen, "FIELD: A Program for Simulating Ultrasound Systems," *Medical and Biological Engineering and Computing*, vol. 34, no. SUPPL. 1, pp. 351–352, 1996.
- [9] J. A. Jensen and N. B. Svendsen, "Calculation of Pressure Fields from Arbitrarily," *IEEE Trans. Ultrason., Ferroelectr., Freq. Control*, vol. 39, no. 2, pp. 262–267, 1992.
- [10] H. C. So, "Source Localization: Algorithms and Analysis," in *Handbook of Position Location: Theory, Practice, and Advances*, 2011, ch. 2, pp. 25–66.
- [11] G. C. Carter, "Coherence and time delay estimation," *Proceedings of the IEEE*, vol. 75, no. 2, pp. 236–255, 1987.